J Mater Sci: Mater Electron (2012) 23:1569–1574
DOI 10.1007/s10854-012-0630-z

Characterization deep boron diffused p^{++} silicon layer

Shankar Dutta · Akhilesh Pandey · G. Saxena · R. Raman · A. Dhaul · Ramjay Pal · Ratnamala Chatterjee

Received: 16 December 2011 / Accepted: 18 January 2012 / Published online: 2 February 2012
© Springer Science+Business Media, LLC 2012

Abstract In recent years the boron impurity-based dissolved wafer process has been repeatedly demonstrated as a powerful tool for forming single crystal Si microstructures. However, there is very little report on detailed characterization of the deep boron diffused silicon layer. This paper presents the optimization of deep boron diffused p^{++} silicon layer (>10 μm thick) of boron concentration above 5×10^{19} atoms/cm^3. Detailed characterization of the p^{++} silicon layers, by using high resolution x-ray diffraction, secondary ion mass spectrometry, secondary electron micrograph are done. The optical behaviour of the p^{++} layers in mid-IR range is also carried out. The stress generated due to the deep diffusion is estimated to be 822 MPa by Raman spectroscopy.

1 Introduction

Heavily boron-doped silicon microstructures fabricated using deep-boron diffusion and boron etch-stop techniques have been widely used in a variety of integrated sensors and actuators [1–4]. These techniques offer high reproducibility, excellent uniformity, high yield, and ease of processing in fabricating a number of microstructures, diaphragms, doubly clamped beams, and cantilever beams of various shapes and dimensions [4–10]. For many applications, having knowledge of the mechanical properties such as Young's modulus, intrinsic stress and fracture stress of thin films is very important in calculating and characterizing the response parameters of sensors and actuators that utilize them.

Since the structural material is heavily boron doped single crystal Si (p^{++} Si), this process is also attractive for resonant devices such as gyroscopes because of the very high mechanical quality factors that can be achieved. Many of the devices that have been developed incorporate an insulating glass substrate to which the silicon microstructures are bonded [4, 5, 11, 12].

Majority of the previously published papers discussed the characterization of p^{++} silicon layer (concentration $>5 \times 10^{19}$ atoms/cm^3) of thickness 1–5 μm [2, 3, 5, 8, 9, 11, 12]. There are also a number of papers which reported the p^{++} layer thickness above 10 μm or more, but discussed only about the boron concentrations and its' etch stop properties in aqueous alkaline solutions [6, 10, 13–17]. Since stress plays an important role for micro-electro-mechanical system (MEMS) device fabrication, our interest is to see the stress behaviour of highly boron doped silicon layers. Moreover, details characterizations of the deep boron diffused layers may also more enlighten the field of MEMS device physics and their applications. However, only a few papers are available related to the tensile stress generated during the boron diffusion process [2, 18].

In this paper we attempted to characterize the deep boron diffused p^{++} silicon layer (>10 μm thick) of boron concentration above 5×10^{19} atoms/cm^3. This paper reports the optimization of the p^{++} silicon layer formation by deep diffusion. Detailed characterization of the p^{++} silicon layers, by using high resolution x-ray diffraction (HRXRD), secondary ion mass spectrometry (SIMS), secondary electron micrograph (SEM) are reported in this paper. The behaviour of the p^{++} layers under mid infrared (FTIR) is

S. Dutta (✉) · A. Pandey · G. Saxena · R. Raman · A. Dhaul · R. Pal
Solid State Physics Laboratory, DRDO, Lucknow Road, Timarpur, Delhi 110054, India
e-mail: shankardutta77@gmail.com

R. Chatterjee
Department of Physics, IIT Delhi, Hauz Khas, New Delhi 110016, India

also studied. The Raman spectroscopy is used to estimate the residual stress generated during the diffusion process.

2 Experimental

Czocharlski grown 2 in. n type, <100> oriented, 1–10 Ω-cm resistivity silicon wafers are used throughout this study. Standard silicon cleaning steps are followed prior to the high temperature diffusion process. The diffusion experiments are done in a three zone horizontal furnace. The Boro-Disc™ wafers are used as the source for boron dopants. The diffusion experiments were carried out at 1,150 and 1,175 °C in a mixture of nitrogen and oxygen environment. The boro-silicate glass generated during the pre-deposition was kept intact during the drive-in process. This helps to maintain the surface concentration. The drive-in of the samples was done for 10 h. The detail parameters of the diffusion experiments are tabulated in Table 1. Finally, a low temperature (950 °C) wet oxidation for 30 min was done so that the doped oxide, generated during such a prolonged diffusion process, can easily be removed.

Depth profiling of the samples was carried out using a CAMECA IMS 7F secondary ion mass spectrometer (SIMS). An O_2^+ primary ion beam with impact energy of 5 keV and a current of approximately 300 nA was used to raster 250 μm × 250 μm of the sample surface. The secondary ions were collected from a 100 μm dia circular central region of the rastered area to ensure uniformity of sampling depth by using only the flat bottom area of the sputtered out craters. These were then collected and detected using electron multiplier.

The X-ray rocking curve measurements were performed using the PANalytical PW 3050/65 X-Pert Pro MRD HRXRD system with $CuK_{\alpha 1}$ radiations using Bertels-type 4 bounce 4-crystal Ge (220) mono-chromater. The reciprocal space mapping was performed in HRXRD system in triple axis configuration. In this configuration an analyzer crystal Ge (220) was kept in front of the detector in the diffracted beam path.

The diffused samples were studied by using the FTIR VARIAN (Model 670) in transmission and reflection mode in Mid IR region (400–6,000 cm^{-1}). Microscopic studies were carried out by Field-Emission Scanning Electron Microscopy (FE-SEM) (SUPRA-50). Raman Spectroscopy was carried out by Jobin–Yvon Raman Spectrometer (Model no. T64000).

3 Results and discussion

The SIMS profiles of the p^{++} silicon layers are shown in Fig. 1. From the figure it is quite clear that, for 5 h pre-deposition followed by 10 h drive-in in 2 l/min nitrogen (with 20% oxygen) environment yields a p^{++} silicon layer of ~12 μm depth with boron concentration ~5 × 10^{19} atoms/cc or more (sample D). As we are concentrating ourselves only on the properties of p^{++} silicon layer of thickness >10 μm and having boron concentration of more than 5 × 10^{19} atoms/cc, only sample D is further characterized. In the present paper we are concentrating on p^{++} silicon layer of thickness >10 μm and having boron concentration of ≥5 × 10^{19} atoms/cc, so further studies are made on these samples.

3.1 XRD study

It is well known that the dopants—like boron appear to have their diffusion coefficients enhanced when the surface of the

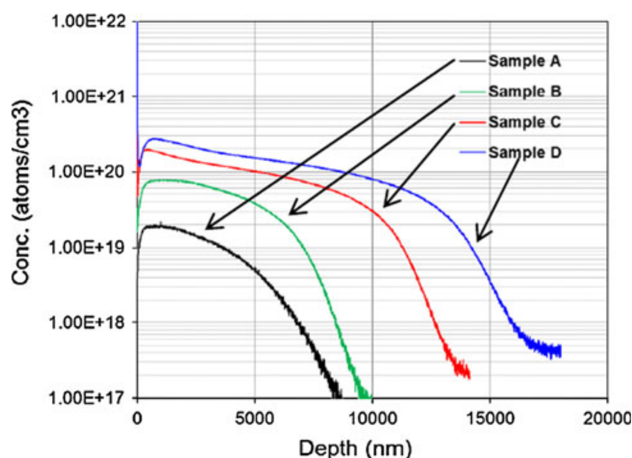

Fig. 1 SIMS profile boron in silicon samples

Table 1 Parameters for diffusion experiments

Sample	Pre-deposition		Drive-in		Nitrogen flow (l/min)	Oxygen flow (ml/min)
	Time (h)	Temperature (°C)	Time (h)	Temperature (°C)		
Sample A	0.5	1,150	10	1,150	2	20
Sample B	1.5	1,175	10	1,175	2	20
Sample C	5	1,175	10	1,175	2	50
Sample D	5	1,175	10	1,175	2	200

silicon is oxidized [19–21]. This experimental observation is important in explaining the dependence of diffusion coefficient on the point defects caused by the surface oxidation of silicon [21]. Because, during oxidation of silicon, large compressive stress is generated and it can be relieved by formation of silicon interstitials to make space for the oxide.

Figure 2 shows the XRD rocking curve of the p^{++} silicon layer in [004] planes along with the bare silicon curve with the same set of planes. From the XRD curves, one can infer that, there is some tensile strain is generated due to the diffusion of the smaller boron dopants into the silicon crystal. The broad hump appearing at the higher angle (ω) side of the curve is due to the large number of silicon interstitials, displaced during the heavy boron diffusion. Implanted samples generally show this kind of behavior [20]. For the deep boron diffused p^{++} silicon samples, we do not find any previously published report on the rocking curve. From the reports related to implanted samples, it was found that these silicon interstitials generally accumulate along the (113) plane and form ribbon like shape [20]. From this analogy, we also studied the XRD rocking curve of the p^{++} silicon samples along [113] planes, which is shown in Fig. 3. The rocking curve clearly shows the asymmetry in the lower angle side which establishes the occurrence of tensile stress in diffused sample. The full-wave half-maxima (FWHM) of the bare and diffused samples along [113] direction are measured to be 30 arc-sec and 144 arc-sec respectively, which indicate that there are large number of point defects are introduced during diffusion process.

For micromechanical and silicon structures, the state of the intrinsic strain of the thin film used is also very important as this often determines the final physical shape of the microstructures that are released from their host substrate. To visualize the strain generated during the prolonged diffusion process, the reciprocal space mapping

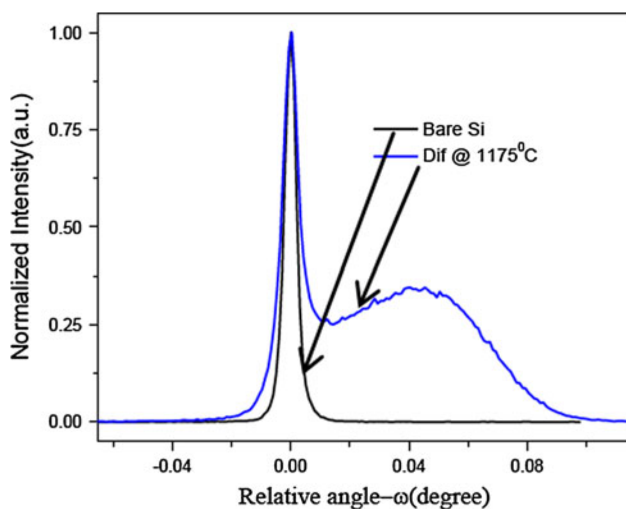

Fig. 2 XRD rocking curve of along [004]

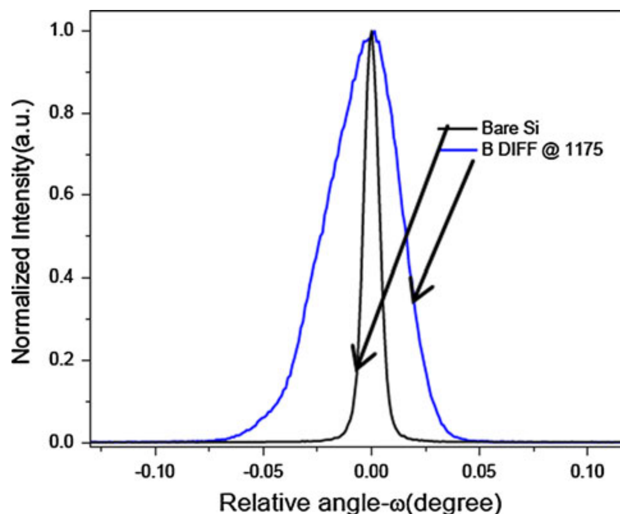

Fig. 3 XRD rocking curve along [113]

(RSM) of the samples were done by HRXRD. The RSM contours for the (113) plane in the Grazing Incidence Geometry is shown in Fig. 4. Here, the RSM contour is showing asymmetry in the lower angle side. This may be due to the generation of tensile strain in silicon lattice after deep boron diffusion.

3.2 FTIR study

The behavior of the p^{++} silicon layer under the mid IR radiations is also studied. The transmittance and reflectance study of the p^{++} silicon sample under IR radiation are shown in Fig. 5. The FTIR transmittance of the bare silicon shows the traditional flat response, as silicon is transparent to mid IR range. The peaks of CO_2 and moisture are appearing in the spectra due to the measurement condition. The p^{++} silicon layer, doped at 1,175 °C, shows zero transmittance at the mid IR range as shown in Fig. 5a. FTIR reflectance graph of the doped and undoped silicon samples are shown in Fig. 5b. One can clearly observe the appearance of Plasma resonance frequency (where, dielectric constant $\varepsilon(\omega)$ becomes zero) in form of reflectance minima above 1,950 cm^{-1} in the deep boron diffused silicon samples. The appearance of plasma resonance frequency occurred due to the incorporation of large number of free charge careers in the diffused sample.

3.3 Raman spectroscopy study

It is important to control mechanical stress induced by processing steps in MEMS manufacturing. The stress can in many cases be monitored using micro-Raman spectroscopy. This technique is rather unique in the sense that it is the only simple, spectroscopic, non-destructive technique that can offer this information.

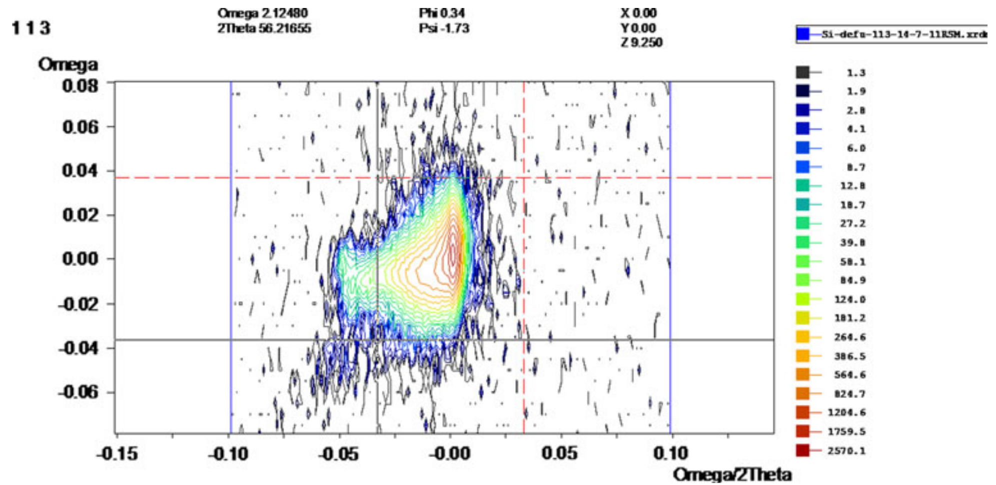

Fig. 4 RSM of p^{++} Si along [113]

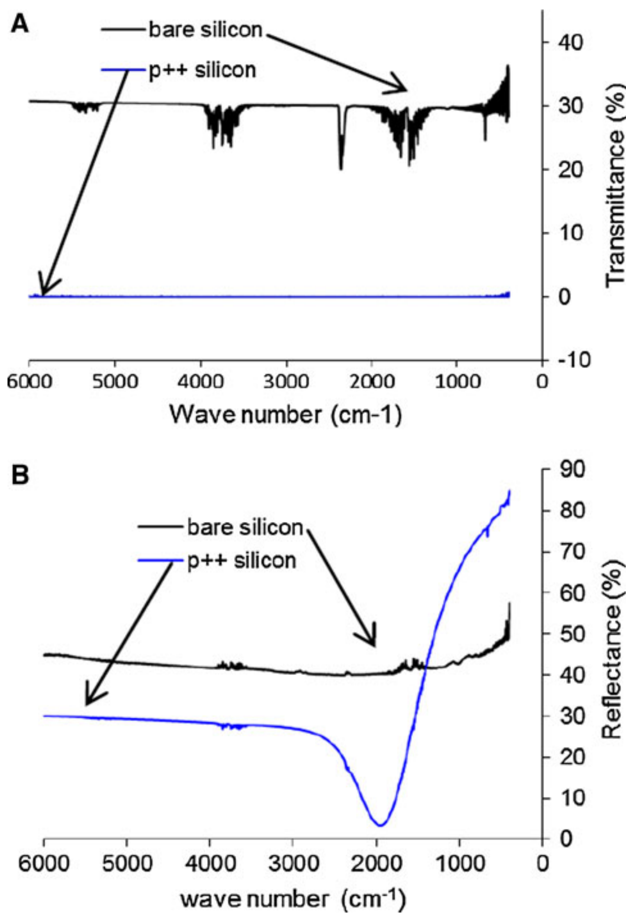

Fig. 5 **a** FTIR (transmittance) study of the p^{++} Si layer. **b** FTIR (reflectance) study of the p^{++} Si layer

Raman spectrum of crystalline silicon, measured using the 457.8 nm line of an argon laser. The Raman spectra of the silicon sample's surface were measured at room temperature before and after deep boron diffusion using a Raman microscope in the backscattering geometry mode. Figure 6 shows a Raman spectrum of the diffused as well

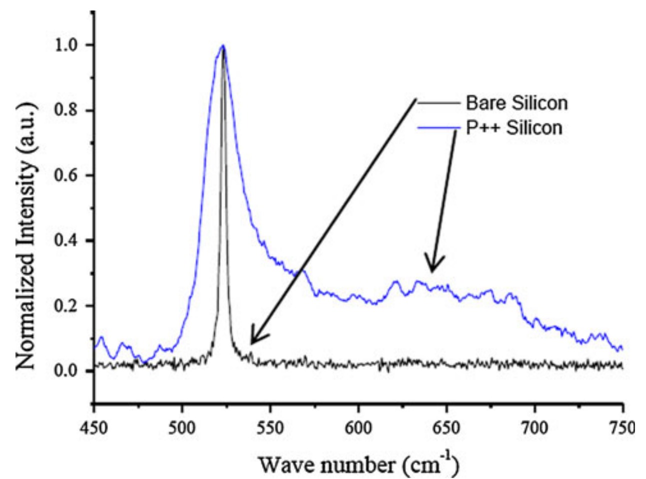

Fig. 6 Raman spectroscopy study of p^{++} silicon layer

as bare silicon samples. The Raman peak corresponding to the bare silicon is appearing at 523.74 cm^{-1}. Generally for the bare silicon Raman peak occurs at $\omega = 521$ cm^{-1}, however, mechanical strain results in a change of this value. The corresponding Raman peak for the deep boron diffused silicon sample is at 521.85 cm^{-1}. By monitoring the shift in the Raman peak before and after the diffusion, one can quantify the stress generated during the diffusion process. The relation between strain or stress and the Raman frequency is rather complex. However, in case of silicon (100) plane, the relation becomes simply linear and can be written as [22]:

$$\mathrm{Stress}(\sigma) \propto \Delta\omega \quad (1)$$

Which can be further simplified to:

$$\sigma = \mathrm{K}\Delta\omega \quad (2)$$

where, K is a constant term, determined by the wavelength of the laser source and the substrate material. For, Silicon, $\mathrm{K} = -435$ MPa cm.

Where, σ be the stress generated and $\Delta\omega$ is the shift in Raman peak. In general, compressive stress will result in an increase of the Raman frequency (wave number), while tensile stress results in a decrease. From the shift in Raman peaks, the estimated tensile stress generated from the diffusion process is 822.15 MPa, i.e. 8.22×10^9 dynes/cm^2. Our measured stress value is quite high compared to the reported values tensile stress by Nazafi (1.83×10^8 dynes/cm^2) [2] and Ning ($>1 \times 10^9$ dynes/cm^2) [18]. This is due to the fact that, our diffused samples have larger diffusion thickness (hence, prolonged diffusion time) compared to both of Nazafi and Ning. To relieve these high levels of stress, the silicon crystal yields and may generate dislocations that may degrade MEMS devices performances.

Moreover, from the Fig. 6, one can clearly see the broadening of the Raman peak along with the broad hump in p^{++} silicon sample. The measured values of FWHM before and after the diffusion process are 4 and 27 cm^{-1} respectively. This is may be due to the presence of large number silicon interstitials generated during the prolonged diffusion process.

3.4 SEM study

It is well known that boron is a substitution dopant in silicon. Figures 7 and 8 show the SEM pictures of the surfaces of the bare and p^{++} silicon layers respectively. As the smaller boron atom displaces the silicon atom, and exerts a tensile stress into the crystal lattice. Due to the incorporation of very high levels of boron (concentration: 5×10^{19} atoms/cc or more), large residual stresses are generated, which may affect the MEMS device performance. To relieve these high levels of stress, dislocations may be generated in the silicon crystal and create damages in silicon wafer surface. From the Fig. 8, one can clearly see that due to the heavy boron diffusion the silicon surface get damaged. The residual stress resulting is dependent on the gradient and maximum magnitude of the boron dopant profile as well as the depth (thickness) of the layer. Form SIMS profile one can see that the boron dopant concentration is not uniform (gradually decreasing) along the depth; so the stress distribution also varies with depth. Figure 9 shows the SEM cross-section of the p^{++} silicon layer. The light-grey region in the picture is the cross-section of the p^{++} silicon layer and dark-grey is corresponding to bulk of the silicon. One can easily see that, there is no boron-oxide/silicide phase is generated during deep boron diffusion.

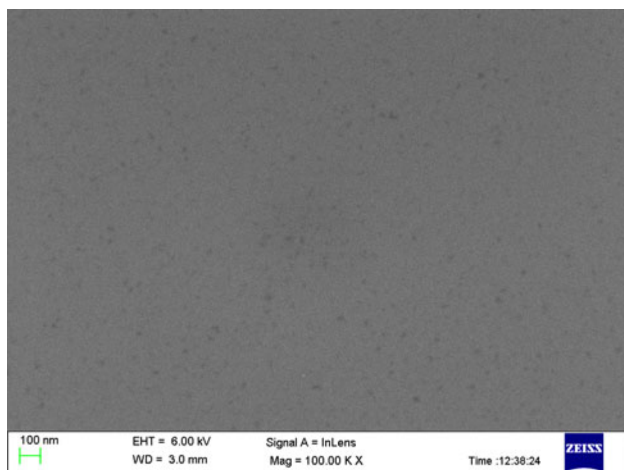

Fig. 7 SEM image of bare silicon

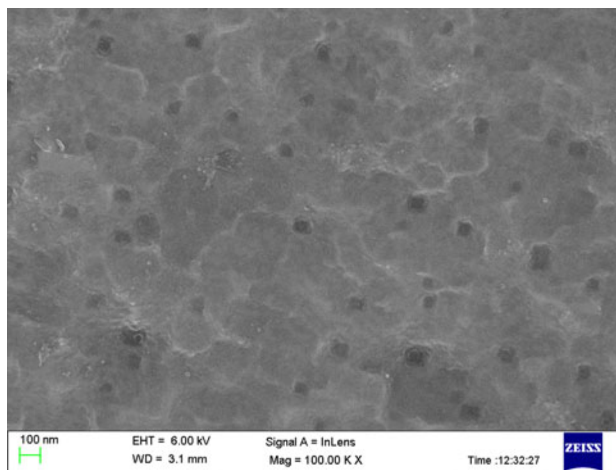

Fig. 8 SEM image of the p^{++} silicon

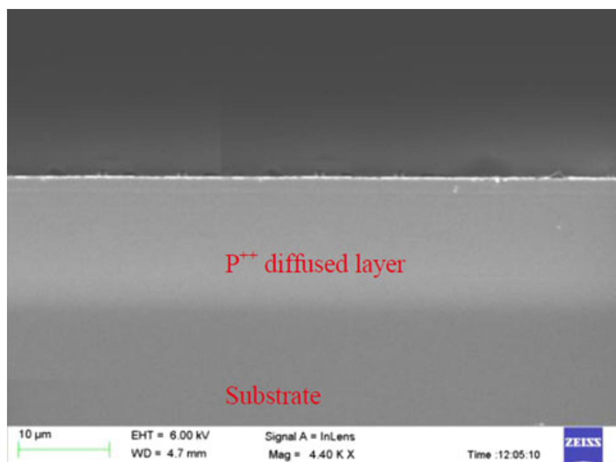

Fig. 9 SEM cross-section of the diffused layer

4 Conclusion

Deep boron diffused p^{++} silicon layer is an important process step to define the thickness of the bulk

micromachined silicon microstructures. In this paper we presented the optimization results (SIMS) of p^{++} silicon layers, having concentrations of 5×10^{19} atoms/cc or more with 10 μm or more depth. The diffused samples were characterized in detail by different techniques such as XRD, FTIR, Raman Spectroscopy, and SEM. The spreading of XRD rocking curve in lower angle side proved the presence of tensile stress due to the incorporation of the large number of boron atoms. The dislodged silicon atoms formed silicon interstitials and is represented by the broad hump in the rocking curve at higher angle side. FTIR study showed that incorporation of p^{++} diffused layer yield zero transmittance in the mid IR range. This can be used for fabrication of IR (Mid) Grating by creating doped (p^{++}) and un-doped regions on the silicon surface. The reflectance spectra of mid IR showed the appearance of plasma resonance frequency above 1,950 cm^{-1}, like free electron gas (metal), in the p^{++} diffused samples. However, due to these levels of boron concentration, high levels of residual stress are generated in these structures, which may affect the MEMS device performance. In our experiments, the deep boron diffused sample is generating a tensile stress $\sim$822 MPa, which is quite large keeping in view of the microns scale MEMS device geometry. This is because mechanical stress has always been an important concern for MEMS-processing and reliability engineers. The mechanical stress can have direct or indirect effects on the functioning and reliability of the device, and cause different failure modes, such as dislocations, fracture of MEMS structures etc.

Acknowledgments Authors would like to thank Director, Solid State Physics Laboratory, for his kind permission to publish this work. Help from other colleagues are also acknowledged.

References

1. G.L. Vick, K.M. Whittle, J. Electrochem. Soc. Solid State Sci. **116**, 1142 (1969)
2. K. Najafi, K. Suzuki, Thin Solid Films **181**, 251 (1989)
3. J.M. Karl, Y.B. Gianchandani, K. Najafi, Semicond. Technol. Sci. **2**, 273 (2002)
4. K.D. Wise, K. Najafi, Science **254**, 1335 (1991)
5. Y. Zhang, K.D. Wise, IEEE Jr. MEMS **3**, 59 (1994)
6. J.W. Weigold, W.H. Juan, S.W. Pang, J. Vac. Sci. Technol. B **15**, 267 (1997)
7. J. Hsieh, W. Fang, J. Micromech. Microeng. **12**, 574 (2002)
8. C.S. Lee, C.H. Han, Sens. Actuators A **88**, 87 (2001)
9. C. Iliescu, M. Avram, J. Miao, F.E.H. Tay, IEEE International Semiconductor Conference **281** (2003)
10. T. Ohno, S. Tanaka, M. Esashi, IEEJ Trans. Electr. Electron. Eng. **5**, 493 (2010)
11. Y.Y. Chen, C.N. Chen, W.C. Huang, IEEE Proceedings of the 3rd International Conferences on Nano/Molecular Medicine and Engineering, Taiwan **180** (2009)
12. C. Huang, K. Najafi, IEEE Jr. MEMS **10**, 532 (2001)
13. S.E. Alper, Y. Temiz, T. Akin, IEEE Jr. MEMS **17**, 1418 (2008)
14. S. Dutta, R. Pal, P. Kumar, O.P. Hooda, J. Singh, Shaveta, G. Saxena, P. Datta, R. Chatterjee, Sens. Trans. J. **111**, 18 (2009)
15. M.E. Merriam, S. Dehmel, O. Srivannavit, S.E. Shore, K.D. Wise, IEEE Trans. Biomed. Eng. **58**, 397 (2011)
16. M.E. Merriam, O. Srivannavit, M.N. Gulari, K.D. Wise, IEEE Jr. MEMS **20**, 594 (2011)
17. H. Seidel, L. Csepregi, A. Heuberger, A. Baumgartel, J. Electrochem. Soc. **137**, 3612 (1990)
18. X.J. Ning, J. Electrochem. Soc. **143**, 3389 (1996)
19. I. Ban, M.C. Oztiirk, E. Demirlioglu, IEEE Proceedings of the 11th International Conferences on Ion Implantation Technology **740** (1996)
20. J.D. Plummer, M. Deal, P.B. Griffin, *Silicon VLSI Technology—Fundamentals, Practice and Modelling* (Prentice Hall, New Jersey, 2000)
21. R.B. Fair, A.F.W. Willoughby, in *Impurity Doping Processes in Silicon*, ed. by F.F.Y. Wang. Materials and Processing Theory and Practices, vol. 2, Chap. 7, (North Holland, 1981)
22. I.D. Wolf, Spectroscopy Europe 15/2 6 (2003)